Influence of Crack Morphology and its distribution on Stress magnification of AA2024-T3

Zaigham Saeed Toor

***Abstract*—The effect of crack shape, size and its distribution on the stress magnification of Aluminum alloy AA2024-T3 tensile test specimen was studied using Finite Element Analysis (FEA) approach. A defect free neat reference sample of the alloy was developed as per ASTM-E8 standard using ANSYS Multiphysics. Circular and rectangular cracks of 0.1 inch to 0.3 inch diameter for circular cracks and 0.1 inch to 0.3 inch wide rectangle having same area as their circular counterparts were incorporated in the reference sample to study influence of crack morphology on stress magnification, while three 0.1 inch circular cracks were distributed diagonally on the reference specimen to study the influence of crack distribution, with separate simulations for each specimen. Each specimen was subjected to a fixed support and a tensile load on opposite end was applied to stress the material to Ultimate tensile strength. 24%, 13% and 26% increase in stress magnification was observed for 0.1 inch, 0.2inch and 0.3-inch rectangular cracks of same area as their circular crack counterparts while 21% reduction in stress magnification was observed by distributing same number of cracks from concentrated to diagonal distribution.**

***Index Terms*— Aerospace Materials, Material Testing, Finite Element Analysis, Stress Magnification**

I. Introduction

Aluminum, aluminum alloys and aluminum based composites are very popular in the field of aircraft and aerospace design[1, 2]. This can be related to the fact that they provide the designer with diverse properties such as high specific strength, low cost, ease of manufacturing, weight reduction, corrosion resistance and good machinability[3-6]. A lot of research has been done on the experimental aspects of various materials but the computational materials science or Finite Element Analysis is an emerging research trend[7-13].

Finite Element Analysis (FEA) is a computer based technique employed using computational software such as MATLAB, ANSYS, COSMOL and many others to model and simulate various material scenarios by incorporating the required boundary conditions such as material properties, environment, design and meshing[14-16]. Tensile testing is a common type of mechanical testing in which a specimen of the material to be tested is prepared according to the international standards available such as American Society for Testing and Materials (ASTM)[17], clamped in a Universal Testing Machine (UTM)[18] and then subjected to tensile loading until failure.

Date Received: 1st May 2020.
Zaigham Saeed Toor is a Materials Science & Engineering graduate from Institute of Space Technology (IST), Islamabad, Pakistan
Corresponding author: zaighamtoor93@gmail.com

This generates a stress-strain curve of the tested material that helps in developing various material properties such as Modulus of Elasticity, Yield Strength, Ultimate Tensile Strength, Toughness and ductility as shown in Fig 1[19-22].It is also important to mention that Von-Mises stress is the stress type used in FEA of materials that helps in analyzing how a material or assembly will yield or behave plastically under different loading conditions[23-25].

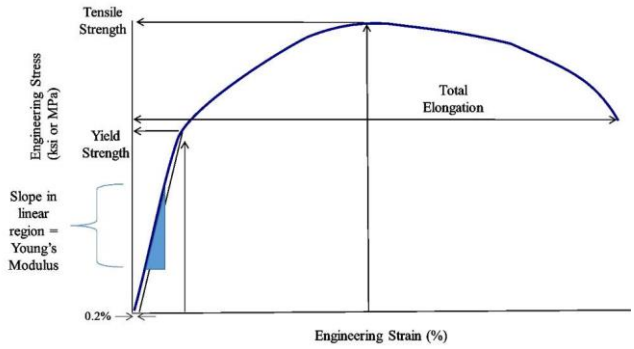

Fig 1: Stress-Strain Curve of a material[22]

Stress concentration factor (K_t) is described as the ratio of the maximum stress generated in a sample due to a crack, hole, cut or any other defect to the stress generated in the same sample at the same load but without any stress risers or defects. Since it is a ratio, it does not have any dimension[26-28]. In order to replace a circular crack with a rectangular crack, we can calculate the area of that circle and replace it with a rectangular crack of the same area[29].

This research focuses on the incorporation of self-induced circular and rectangular cracks of same area and crack size in a defect free specimen using FEA. Distribution of self-induced cracks in a defect free specimen and its corresponding effect on stress magnification is also studied using FEA approach.

II. Experimental Procedure

Static Structural Workbench Module of ANSYS 14.0 Multiphysics was used for Finite Element Analysis (FEA) of Aluminum alloy AA 2024-T3 [14, 15, 30]. Experimental parameters of FEA and material properties are shown in Table I and II respectively. The specimen for testing was developed using American Society of Testing and Materials (ASTM) standard E8[31] having dimensions as shown in Fig 2 and Table III respectively. Nine simulations were performed by changing the crack morphologies, distributions and comparing the corresponding applied loads, total deformation, equivalent total strain and equivalent (von-Mises) stress as shown in Table

IV. All meshing, analysis and solution setting were kept constant.

TABLE I
Experimental Parameters of FEA

Parameters	Values
GEOMETRY	
Unit System	Metric (mm, kg, N, s, mV, mA)
Geometry State	Fully Defined
Type	Design Modeler
Length Unit	Inches
Element Control	Program Controlled
Display Style	Body Color
Bodies/Active Bodies	1
Nodes	12828
Elements	6204
Mesh Metric	None
Use Associativity	Yes
Analysis Type	3D
Stiffness Behavior	Flexible
Assignment	AA202-T3
Non-linear Effects	Yes
Thermal Strain Effects	Yes
MESH	
State	Solved
Physics Preference	Mechanical
Advanced Size Function	Off
Relevance Center	Fine
Element Size	Default
Initial Size Seed	Active Assembly
Smoothing	Medium
Transition	Fast
Span Angle Centre	Coarse
Minimum Edge Length	4.76250 mm
Triangular Surface Mesher	Program Controlled
ANALYSIS & SOLUTION	
Physics Type	Structural
Analysis type	Static Structural
Solver Target	Mechanical APDL
Step Control	1s
Auto Time Stepping	Program Controlled
Solver type	Program Controlled
Weak Springs	Off
Large Deflection	On
Inertia Relief	Off
Support Type	Fixed Support
Load Type	Normal Force (Ramped)
Defined By	Components (X,Y,Z)

In order to study the effect of crack morphology on stress magnification, the first simulation was performed on a neat reference sample of the alloy which was assumed to be free from any defects and cracks as shown in Fig 3. The sample was subjected to a fixed support on one face and on the opposite face tensile load was applied to generate target stress between 483 to 484 MPa, which was very close to the Ultimate Tensile Strength of the alloy as shown in Fig 4. The applied load, total deformation, equivalent total strain and equivalent (von-Mises) stress were recorded in Table V.

TABLE II
Material Data

Parameters	Values
Type	Aluminum Alloy
Designation	2024
Temper Grade	T3
Density	2.78 g/cm^3
Temperature	25°C
Youngs Modulus	73100 MPa
Poisson's Ratio	0.33
Bulk Modulus	71677 MPa
Shear Modulus	27481 MPa
Tensile Yield Strength	345 MPa
Ultimate Tensile Strength	483 MPa
Multilinear Isotropic Hardening	
Stress (MPa)	**Plastic Strain (mm^{-1})**
350	0.004
420	0.01
440	0.015
465	0.02
485	0.025

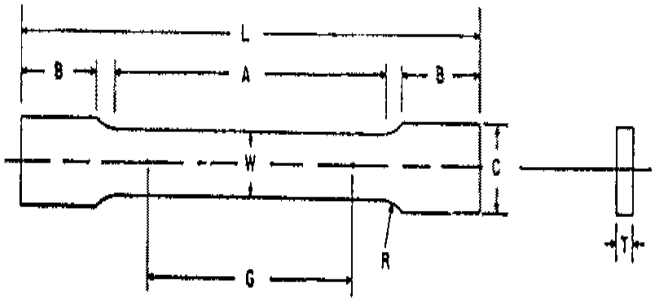

Fig 2: Tensile Test Specimen with permission from ASTM[31]

TABLE III
Specimen Dimensions as per ASTM-E8 Standard[31]

Parameters	Values
Gauge Length (G)	2.0 inches
Width (W)	0.5 inch
Thickness (T)	0.1865 inch
Radius of Fillet (R)	0.5 inch
Overall Length (L)	8.0 inch
Length of reduced section (A)	2.25 inch
Length of grip section (B)	2.0 inch
Width of grip section (C)	0.75 inch

TABLE IV
Parameters for Evaluation of Stress Magnification

Parameters	Units
Applied load (Max)	KN
Total Deformation (Max)	mm
Total Equivalent Strain (Max)	mm^{-1}
Equivalent Von-Mises Stress (Max)	MPa

TABLE V
Results of First Simulation

Parameters	Units
Applied load (Max)	28 KN
Total Deformation (Max)	3.3 mm
Total Equivalent Strain (Max)	0.033 mm^{-1}
Equivalent Von-Mises Stress (Max)	484 MPa

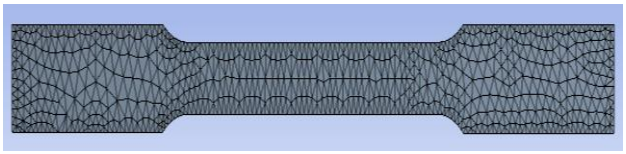

Fig 3: Meshed Reference sample

The second simulation was performed by creating a circular crack hole of 0.1-inch diameter in center of the neat sample as shown in Fig 5. The sample was then subjected to the same tensile loading to generate the target stress as shown in Fig 6 and the corresponding values of applied load, total deformation, equivalent total strain and equivalent (von-Mises) stress were recorded in Table VI.

Fig 4: Reference sample under stress

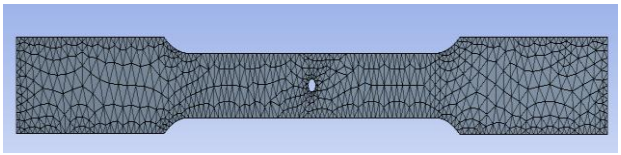

Fig 5: 0.1-inch center drilled meshed specimen

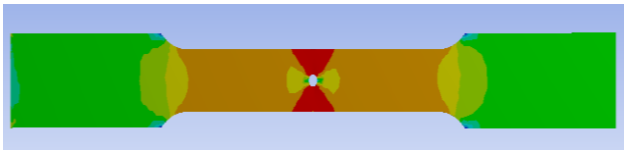

Fig 6: 0.1-inch center drilled specimen under stress

TABLE VI
Results of Second Simulation

Parameters	Units
Applied load (Max)	23.9 KN
Total Deformation (Max)	1.8 mm
Total Equivalent Strain (Max)	0.18 mm^{-1}
Equivalent Von-Mises Stress (Max)	484 MPa

The third simulation was performed by creating a circular crack hole of 0.2-inch diameter in center of the neat sample as shown in Fig 7. The sample was then subjected to the same tensile loading to generate the target stress as shown in Fig 8 and the corresponding values of applied load, total deformation, equivalent total strain and equivalent (von-Mises) stress were recorded in Table VII.

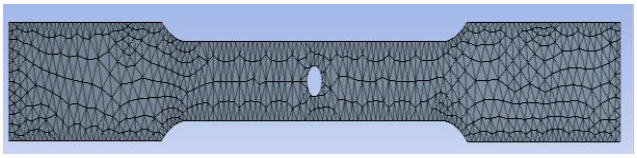

Fig 7: 0.2-inch center drilled meshed specimen

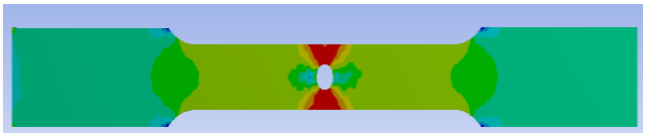

Fig 8: 0.2-inch center drilled specimen under stress

The fourth simulation was performed by creating a circular crack hole of 0.3-inch diameter in center of the neat sample as shown in Fig 9. The sample was then subjected to the same tensile loading to generate the target stress as shown in Fig 10 and the corresponding values of applied load, total deformation, equivalent total strain and equivalent (von-Mises) stress were recorded in Table VIII.

TABLE VII
Results of Third Simulation

Parameters	Units
Applied load (Max)	17.9 KN
Total Deformation (Max)	1.0 mm
Total Equivalent Strain (Max)	0.12 mm^{-1}
Equivalent Von-Mises Stress (Max)	484 MPa

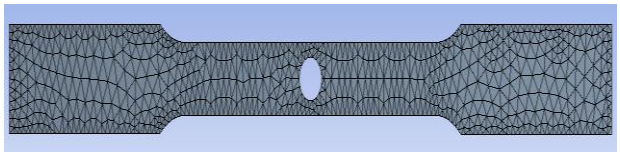

Fig 9: 0.3-inch center drilled meshed specimen

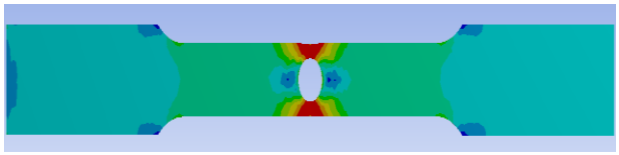

Fig 10: 0.3-inch center drilled specimen under stress

TABLE VIII
Results of Fourth Simulation

Parameters	Units
Applied load (Max)	11.92 KN
Total Deformation (Max)	0.76 mm
Total Equivalent Strain (Max)	0.088 mm^{-1}
Equivalent Von-Mises Stress (Max)	484 MPa

The fifth simulation was performed by creating a rectangular crack of 0.1-inch width and of the same area as the circular crack of 0.1-inch diameter in center of the neat sample as shown in Fig 11 so that area of the crack is maintained and only morphology is changed. The sample was then subjected to the same tensile loading to generate the target stress as shown in Fig 12 and the corresponding values of applied load, total deformation, equivalent total strain and equivalent (von-Mises) stress were recorded in Table IX.

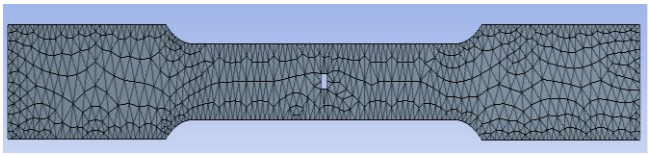

Fig 11: 0.1-inch Rectangular crack meshed specimen

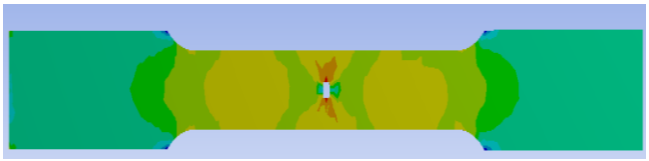

Fig 12: 0.1-inch Rectangular crack specimen under stress

TABLE IX
Results of Fifth Simulation

Parameters	Units
Applied load (Max)	20 KN
Total Deformation (Max)	1.02 mm
Total Equivalent Strain (Max)	0.036 mm^{-1}
Equivalent Von-Mises Stress (Max)	484 MPa

The sixth simulation was performed by creating a rectangular crack of 0.2-inch width and of the same area as the circular crack of 0.2-inch diameter in center of the neat sample as shown in Fig 13. The sample was then subjected to the same tensile loading to generate the target stress as shown in Fig 14 and the corresponding values of applied load, total deformation, equivalent total strain and equivalent (von-Mises) stress were recorded in Table X.

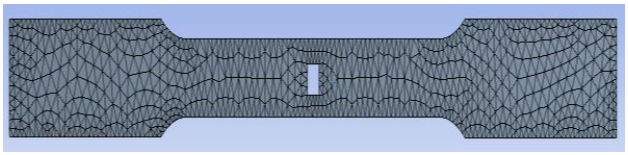

Fig 13: 0.2-inch Rectangular crack meshed specimen

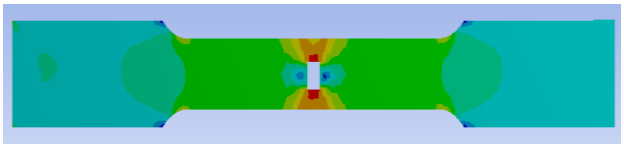

Fig 14: 0.2-inch Rectangular crack specimen under stress

TABLE X
Results of Sixth Simulation

Parameters	Units
Applied load (Max)	15.5 KN
Total Deformation (Max)	0.75 mm
Total Equivalent Strain (Max)	0.032 mm^{-1}
Equivalent Von-Mises Stress (Max)	484 MPa

The seventh simulation was performed by creating a rectangular crack of 0.3-inch width and of the same area as the circular crack of 0.3-inch diameter in center of the neat sample as shown in Fig 15. The sample was then subjected to the same tensile loading to generate the target stress as shown in Fig 16 and the corresponding values of applied load, total deformation, equivalent total strain and equivalent (von-Mises) stress were recorded in Table XI.

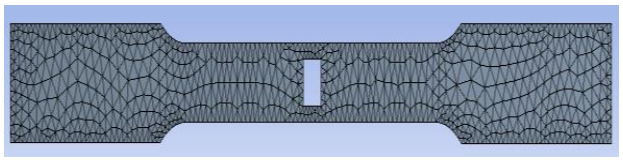

Fig 15: 0.3-inch Rectangular crack meshed specimen

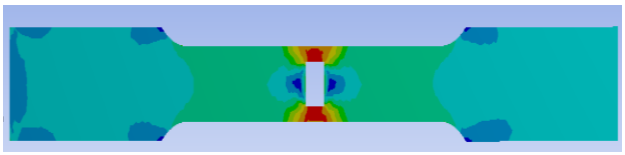

Fig 16: 0.3-inch Rectangular crack specimen under stress

TABLE XI
Results of Seventh Simulation

Parameters	Units
Applied load (Max)	10.8 KN
Total Deformation (Max)	0.63 mm
Total Equivalent Strain (Max)	0.031 mm^{-1}
Equivalent Von-Mises Stress (Max)	484 MPa

In order to study the effect of crack morphology, the eighth simulation was performed by creating three 0.1-inch diameter circular cracks in center of the neat sample, normal to the loading direction as shown in Fig 17. The sample was then subjected to the same tensile loading to generate the target stress as shown in Fig 18 and the corresponding values of applied load, total deformation, equivalent total strain and equivalent (von-Mises) stress were recorded in Table XII.

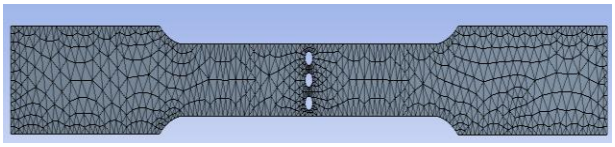

Fig 17: 0.1-inch three concentrated center drills meshed specimen

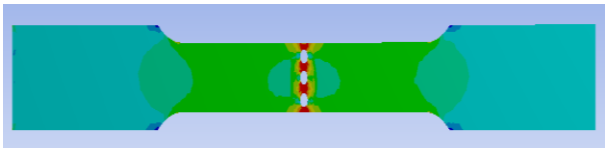

Fig 18: 0.1-inch three center drills specimen under stress

TABLE XII
Results of Eighth Simulation

Parameters	Units
Applied load (Max)	13.9 KN
Total Deformation (Max)	0.67 mm
Total Equivalent Strain (Max)	0.1 mm^{-1}
Equivalent Von-Mises Stress (Max)	484 MPa

The ninth simulation was performed by distributing three 0.1-inch diameter circular cracks in a diagonal pattern to achieve maximum crack interspacing on the neat sample as shown in Fig 19. The sample was then subjected to the same tensile loading to generate the target stress as shown in Fig 20 and the corresponding values of applied load, total deformation, equivalent total strain and equivalent (von-Mises) stress were recorded in Table XIII.

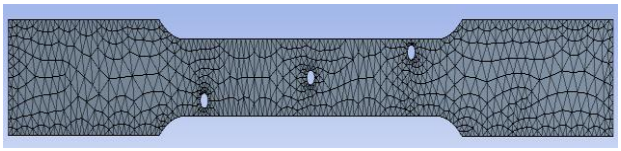

Fig 19: 0.1-inch three diagonally center drills meshed specimen

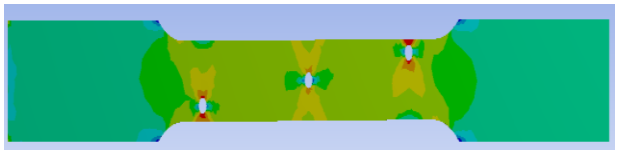

Fig 20. 0.1-inch three diagonally distributed specimen under stress

TABLE XIII
Results of Ninth Simulation

Parameters	Units
Applied load (Max)	18 KN
Total Deformation (Max)	0.85 mm
Total Equivalent Strain (Max)	0.083 mm^{-1}
Equivalent Von-Mises Stress (Max)	484 MPa

Stress magnification was calculated form ratio method[26] and the corresponding plots of stress concentration factors were plotted for both circular and rectangular geometries as shown in Table XIV and Fig 21. Diameter of circular cracks and height of rectangular cracks to width of specimen ratios were used to compare the effect of crack morphologies. It was observed that the stress magnification and concentration factors for the rectangular cracks were higher than their circular counterparts. This can be related to the increased number of stress risers in the rectangular cracks in the form of sharp corners[32].

TABLE XIV
Calculated Stress Concentration Factors at σ_{max} =484 MPa

Crack Type	Crack diameter/Width	Reference Stress (σ_{ref}) (MPa)	Stress Concentration Factor ($K_t = \sigma_{max}/\sigma_{ref}$)
Circular	0.1	421	1.14
	0.2	345	1.40
	0.3	258	1.88
Rectangular	0.1	350	1.38
	0.2	317	1.52
	0.3	234	2.06
Concentrated Circular	0.1	301	1.60
Distributed Circular	0.1	346	1.39

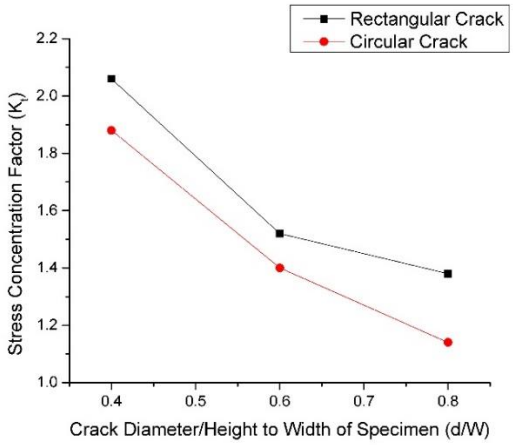

Fig 21. Comparison of Crack morphology in terms of K_t

III. Results and Discussions

The stress-strain curve of the neat sample is plotted in Fig 22. It was observed from Table V that the target stress was achieved at a load of 28KN and a uniform stress distribution along the gauge length was observed as shown in Fig 4.

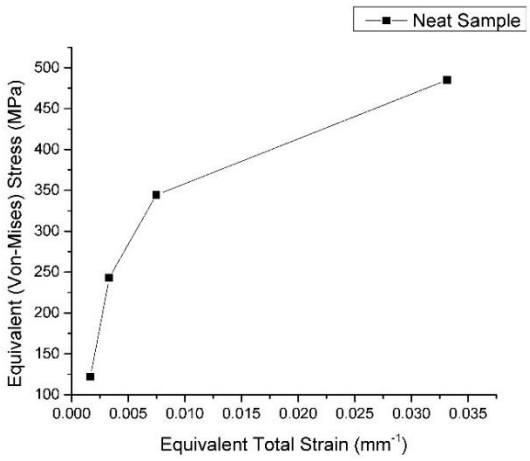

Fig 22: Stress-Strain curve of reference sample

The stress-strain curve of 0.1-inch center drilled circular crack sample is plotted in Fig 23. It was observed from Table VI that the target stress was achieved at a load of 23.9KN and a stress magnification of 14% was developed in which the major stress concentration was observed around the circle as shown in Fig 6. A 55% reduction in total deformation and an increase of 81% in the equivalent total strain was observed in comparison to the reference sample.

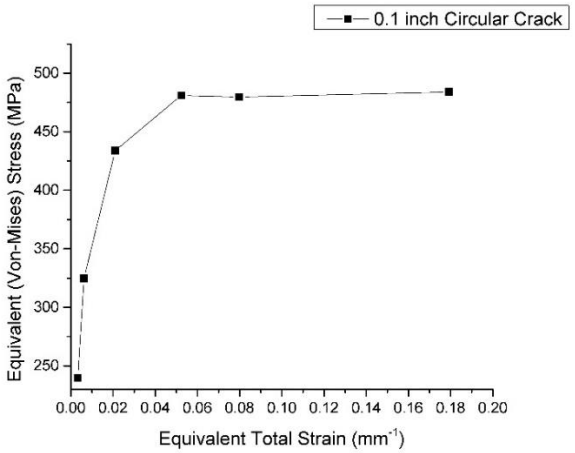

Fig 23: Stress-Strain curve of 0.1-inch center drilled circular crack

The stress-strain curve of 0.2-inch center drilled circular crack sample is shown in Fig 24. It was observed from Table VII that the target stress was achieved at a load of 17.9KN and a stress magnification of 40% was developed in which the major stress concentration was observed around the circle as shown in Fig 8. A 69% reduction in total deformation and an increase of 72% in the equivalent total strain was observed in comparison to the reference sample.

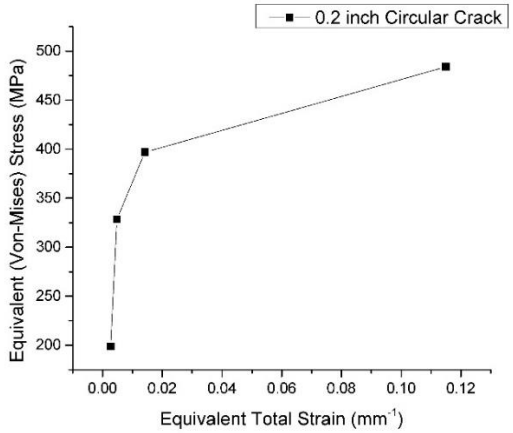

Fig 24: Stress-Strain curve of 0.2-inch center drilled circular crack

The stress-strain curve of 0.3-inch center drilled circular crack sample is plotted in Fig 25. It was observed from Table VIII that the target stress was achieved at a load of 11.92KN and a stress magnification of 80% was developed in which the major stress concentration was observed around the circle as shown in Fig X. A 77% reduction in total deformation and an increase of 63% in the equivalent total strain was observed in comparison to the reference sample.

The stress-strain curve of 0.1-inch center rectangular crack sample is plotted in Fig 26. It was observed from Table IX that the target stress was achieved at a load of 20KN and a stress magnification of 38% was developed in which the major stress concentration was observed around the corners and center longitudinal axis as shown in Fig 12. A 69% reduction in total

deformation and an increase of 8.3% in the equivalent total strain was observed in comparison to the reference sample.

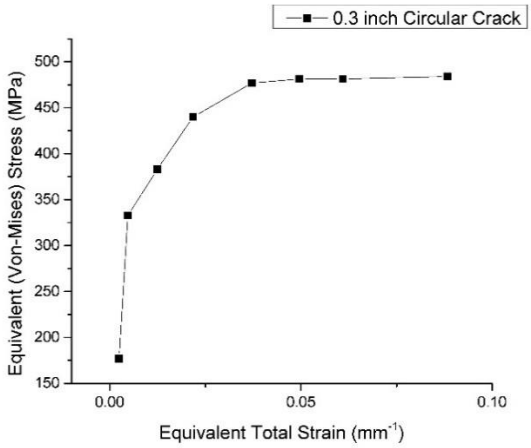

Fig 25: Stress-Strain curve of 0.3-inch center drilled circular crack

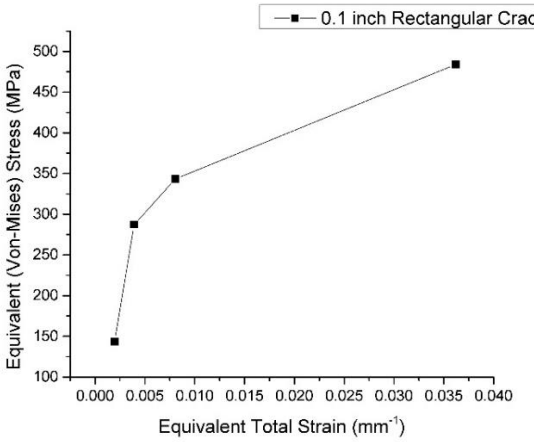

Fig 26: Stress-Strain curve of 0.1-inch Rectangular crack

The stress-strain curve of 0.2-inch center rectangular crack sample is plotted in Fig 27. It was observed from Table X that the target stress achieved was achieved at a load of 15.5KN and a stress magnification of 52% was developed in which the major stress concentration was observed around the corners and center longitudinal axis as shown in Fig 14. A 69% reduction in total deformation and an increase of 8.3% in the equivalent total strain was observed in comparison to the reference sample.

The stress-strain curve of 0.3-inch center rectangular crack sample is shown in Fig 28. It was observed from Table 11 that the target stress achieved was achieved at a load of 10.8KN and a stress magnification of 106% was developed in which the major stress concentration was observed around the corners and center longitudinal axis as shown in Fig 16. An 81% reduction in total deformation and an increase of 3% in the equivalent total strain was observed in comparison to the reference sample.

The stress-strain curve of concentrated three 0.1-inch diameter circular cracks in center of the sample along the y-axis is shown in Fig 29. It was observed from Table XII that the target stress was achieved at a load of 13.9KN. Stress magnification of 61% was developed in which the major stress concentration was observed around the circles along the longitudinal axis as shown in Fig 18. An 80% reduction in total deformation and an increase of 67% in the equivalent total strain was observed in comparison to the reference sample.

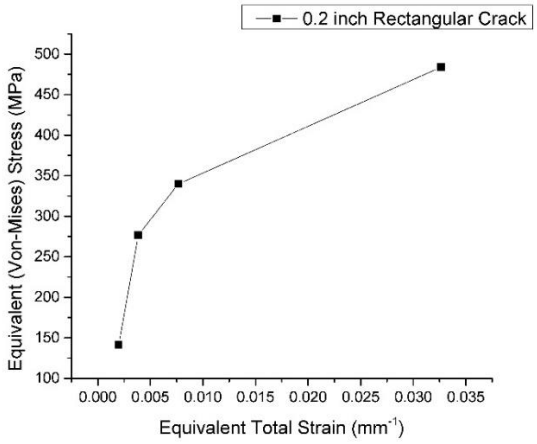

Fig 27: Stress-Strain curve of 0.2-inch Rectangular crack

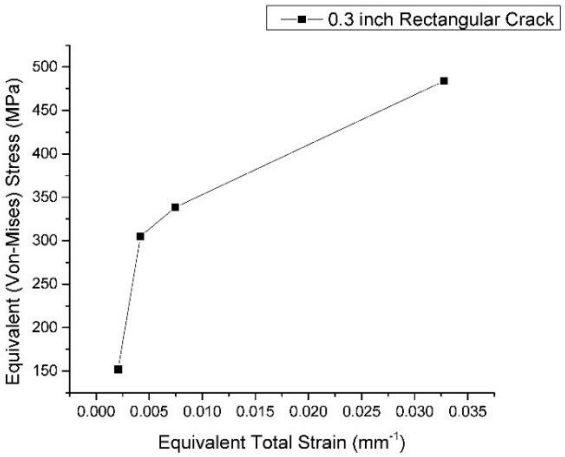

Fig 28: Stress-Strain curve of 0.3-inch Rectangular crack

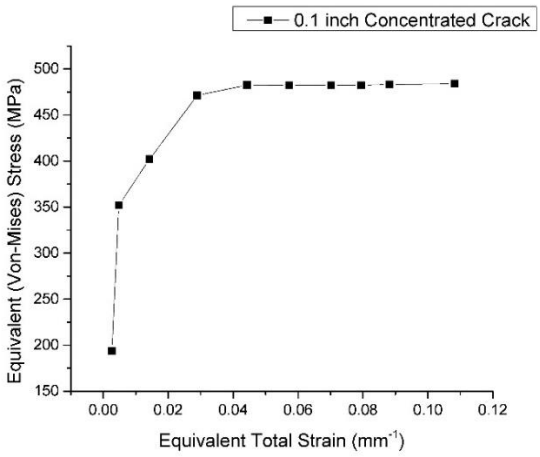

Fig 29: Stress-Strain curve of concentrated three 0.1-inch diameter circular cracks

The stress-strain curve of diagonally distributed three 0.1-inch diameter circular cracks is plotted in Fig 30. It was

observed from Table XIII that the target stress was achieved at a load of 18KN.Stress magnification of 30% was developed in which the major stress concentration was observed around the circles along the longitudinal axis as shown in Fig 20. A 74% reduction in total deformation and an increase of 60% in the equivalent total strain was observed in comparison to the reference sample. As compared to the concentrated crack holes of the same diameter, by distribution of these cracks a reduction of 21% was observed in the stress magnification of the same material sample.

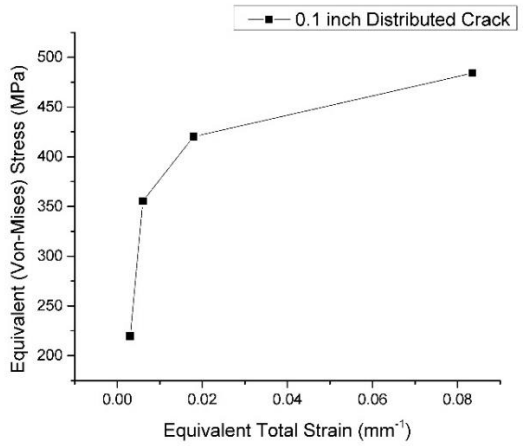

Fig 30: Stress-Strain curve of diagonally distributed three 0.1-inch diameter circular cracks

IV. Conclusion

The research shows that crack morphology can significantly enhance the stress magnification and stress concentration factor in a part or assembly. Analysis reveals 24%, 13% and 26% increase in stress magnification was observed for 0.1-inch, 0.2-inch and 0.3-inch respectively in the rectangular cracks of same area as compared with their circular crack counterparts.

Results further revealed that crack distribution can significantly reduce the stress magnification and stress concentration factor in a part or assembly. A 21% reduction in stress magnification was observed by distributing same number of cracks from concentrated to diagonal distribution.

Analysis of the acquired results reveal that crack size varies directly with stress magnification, while crack distribution varies inversely with stress magnification.

The finite element method is a powerful and versatile tool of researchers and has proved its worth in several fields. Once again it is learnt from the current research work that Finite Element Analysis (FEA) based approach can be further employed to actual material defects such as pores, internal cracks, cuts. The method can be used to develop real time and complex scenarios pertaining to stress related failures of structures, new materials and engineering computational solutions.

References

[1] E. A. Starke and J. T. Staley, "Application of modern aluminum alloys to aircraft," *Progress in Aerospace Sciences*, vol. 32, pp. 131-172, 1996/01/01/ 1996.

[2] M. Shifa, F. Tariq, and A. D. Chandio, "Mechanical and electrical properties of hybrid honeycomb sandwich structure for spacecraft structural applications," *Journal of Sandwich Structures & Materials*, p. 1099636219830783, 2019.

[3] I. Ahmed, S. Ullah, Z. S. Toor, A. Wadood, A. N. Butt, and S. W. Hussain, "Design, Fabrication and Beta testing of Four point Bend Immersion (FPBI) apparatus for the study of Stress Corrosion Cracking (SCC)," in *Student Research Paper Conference (SRPC) Institute of Space Technology (IST), Islamabad, Pakistan*, 2015, pp. 162-166.

[4] Z. S. Toor, I. Ahmed, S. Ullah, A. N. Butt, and S. W. Hussain, "Influence of Ageing time and Stress on Corrosion behavior of AA2024-T6 in saturated NaCl Solution," *Journal of Space Technology (JST)*, vol. 8, pp. 38-44, 2018.

[5] Z. S. Toor, "Space Applications of Composite Materials," *Journal of Space Technology (JST)*, vol. 8, pp. 65-70, 2018.

[6] Z. S. Toor, "Applications of Aluminum-Matrix Composites in Satellite: A Review," *Journal of Space Technology (JST)*, vol. 7, pp. 1-6, 2017.

[7] A. Hassan, M. Muhyuddin, A. Rahman, M. Usman, M. A. Basit, and S. W. Husain, "Improved optical and electrochemical performance of MoS2-incorporated TiO2-PbS nanocomposite for solar paint application," *Journal of Materials Science: Materials in Electronics*, 2020/01/03 2020.

[8] J. U. Rehman and M. H. Chowdhury, "Conventional versus Flexible Substrates for Dye Sensitized and Perovskite Type Photo Voltaic Solar Cells," in *2019 IEEE International Conference on Flexible and Printable Sensors and Systems (FLEPS)*, 2019, pp. 1-3.

[9] J. U. Rehman and M. H. Chowdhury, "Interconnects for Flexible and Printed Electronic Applications," in *2019 IEEE International Conference on Flexible and Printable Sensors and Systems (FLEPS)*, 2019, pp. 1-2.

[10] J. U. Rehman and M. H. Chowdhury, "Super-capacitors and Other Fiber-Shaped Batteries as Energy Storage Devices for Flexible Electronic Devices," in *2019 IEEE International Conference on Flexible and Printable Sensors and Systems (FLEPS)*, 2019, pp. 1-3.

[11] M. Mahmood, H. Ameen, M. F. Zafar, and S. W. Husain, "Development and Characterization of Oxidation Resistant TiC Coating on Graphite," in *2019 16th International Bhurban Conference on Applied Sciences and Technology (IBCAST)*, 2019, pp. 30-34.

[12] A. Safri, J. U. Rehman, S. Shabbir, and S. Hussain, "Bacterial Disinfection Using Polymer Based Hybrids," *Key Engineering Materials*, vol. 778, pp. 331-335, 09/01 2018.

[13] K. I. Khan, M. Latif, M. A. U. Rehman, and S. W. Husain, "Fabrication of Titania Nanotubes by Electrochemical Anodization and their Characterization," in *Student Research Paper Conference (SRPC) Institute of Space Technology (IST), Islamabad, Pakistan*, Islamabad, 2015, pp. 209-211.

[14] J. Kang, W. S. Johnson, and D. A. Clark, "Three-Dimensional Finite Element Analysis of the Cold Expansion of Fastener Holes in Two Aluminum Alloys," *Journal of Engineering Materials and Technology*, vol. 124, pp. 140-145, 2002.

[15] V. Kuppast, *FINITE ELEMENT ANALYSIS OF ALUMINIUM ALLOYS FOR THEIR VIBRATION CHARACTERISTICS* vol. 03, 2014.

[16] M. Shifa, F. Tariq, F. Khan, Z. S. Toor, and R. A. Baloch, "Towards light weight multifunctional hybrid composite housing for satellite electronics," *Materials Research Express*, vol. 6, p. 125629, 2020/01/17 2020.

[17] A. International. (2018). *American Society for Testing and Materials*.

[18] A. DeWolfe. (2012). *What is a Universal Testing Machine?* Available: https://www.admet.com/what-is-a-universal-testing-machine-2/

[19] Y. Chen, A. H. Clausen, O. S. Hopperstad, and M. Langseth, "Stress–strain behaviour of aluminium alloys at a wide range of strain rates," *International Journal of Solids and Structures*, vol. 46, pp. 3825-3835, 2009/10/15/ 2009.

[20] H. J. Liu, H. Fujii, M. Maeda, and K. Nogi, "Tensile properties and fracture locations of friction-stir-welded joints of 2017-T351 aluminum

alloy," *Journal of Materials Processing Technology*, vol. 142, pp. 692-696, 2003/12/10/ 2003.

[21] S. Khokhar, S. W. Husain, T. hussain, M. A. Fakhar, and R. Zafar, "Numerical and experimental analysis of fracture toughness improvement using multi-walled carbon nanotube modified epoxy in fiber metal laminate joints," *Journal of Space Technology (JST)*, vol. 09, pp. 32-37, July, 15,2019 2019.

[22] D. J. Schaeffler. (2015). *The differences between stiffness and strength in metal*. Available: https://www.thefabricator.com/thefabricator/article/metalsmaterials/the-differences-between-stiffness-and-strength-in-metal

[23] K. Farhangdoost and K. Aliakbari, *Comparison between Fatigue Life of Autofrettage and Nonautofrettage Cylinders Using Stress Intensity Factor (K(I))* vol. 452-453, 2010.

[24] Y. Rui, A. Subic, M. Takla, C. Wang, A. Niehoff, N. Hamann, *et al.*, *Biomimetic Design of Lightweight Vehicle Structures Based on Animal Bone Properties* vol. 633, 2013.

[25] L. Engineering. (2012). *What is Von Mises Stress ?* Available: http://www.learnengineering.org/2012/12/what-is-von-mises-stress.htmls

[26] CORROSIONPEDIA. (2018). *Stress Concentration Factor (Kt)*. Available: https://www.corrosionpedia.com/definition/1035/stress-concentration-factor-kt

[27] A. A. Khan and I. R. Memon, "Computation of Critical Crack Sizes for Crack Growth Prediction in Thin Plates," *J. Eng. Appl. Sci.(Peshawar)*, vol. 23, pp. 71-77, 2004.

[28] A. A. Khan, M. Ahmad, and M. A. Ashraf, "Residual Life Estimation of an Attach Angle for a Cargo Aircraft," *Journal of Failure Analysis and Prevention*, vol. 16, pp. 1126 - 1133, 2016.

[29] M. i. Fun. (2018). *Area of Plane Shapes*. Available: https://www.mathsisfun.com/area.html

[30] A. A. S. M. Inc. *Aluminum 2024-T3*.

[31] A. S. f. T. a. M. (ASTM), "Standard Test Methods for Tension Testing of Metallic Materials," ed. West Conshohocken: ASTM International, 1997, p. 21.

[32] S. Hale. (2015). *Why Worry About Sharp Corners and Point Loads?* Available: https://caeai.com/blog/why-worry-about-sharp-corners-and-point-loads